OCT4 impedes cell fate redirection by the melanocyte lineage master regulator MITF

Danna Sheinboim[1,7], Itay Maza[2,7,8], Iris Dror[3,9], Shivang Parikh[1], Vladislav Krupalnik[2], Rachel E Bell[1], Asaf Zviran[2], Yusuke Suita[4], Ofir Hakim[5], Yael Mandel Gutfreund[3], Mehdi Khaled[6], Jacob H Hanna[2,7,*], Carmit Levy[1,7,*]

1. Department of Human Genetics and Biochemistry, Sackler Faculty of Medicine, Tel Aviv University, Tel Aviv 69978, Israel
2. Department of Molecular Genetics, Weizmann Institute, Rehovot, Israel
3. Department of Biology, Technion – Israel Institute of Technology, Haifa 32000, Israel
4. Cutaneous Biology Research Center, Department of Dermatology and MGH Cancer Center, Massachusetts General Hospital, Boston, MA 02114, USA
5. The Mina and Everard Goodman Faculty of Life Sciences Bar-Ilan University, Ramat Gan 5290002, Israel
6. Institut Gustave Roussy, INSERM 1186, Villejuif 94805, France
7. These authors contributed equally to this work
8. Current address: Department of Gastroenterology, Rambam Health Care Campus &Bruce Rappaport School of Medicine, Technion Institute of Technology, Haifa, Israel.
9. Current address: Department of Biological Chemistry, University of California, Los Angeles, CA 90095, USA.

*Correspondence:
carmitlevy@post.tau.ac.il (C.L.); jacob.hanna@weizmann.ac.il (J.H)

Abstract

Ectopic expression of lineage master regulators induces transdifferentiation. Whether cell fate transitions can be induced during various developmental stages has never been systemically examined. Here we discovered that amongst different developmental stages, embryonic stem cells (ESCs) were resistant to cell fate conversion induced by the melanocyte lineage master regulator MITF. We generated a transgenic system and found that in ESCs, the pluripotency master regulator, OCT4, counteracts pro-differentiation induced by MITF by physical interference with MITF transcriptional activity. We further found that ESCs must be released from OCT4-maintained pluripotency prior to ectopically induced differentiation. Moreover, OCT4 induction in various differentiated cells repressed their lineage identity in vivo. Alongside, chromatin architecture combined with ChIP-seq analysis suggested that OCT4 competes with various lineage master regulators for binding promoters and enhancers. Our analysis reveals pluripotency and transdifferentiation regulatory principles and could open new opportunities in the field of regenerative medicine.

Introduction

An ultimate goal of regenerative medicine is to produce functional differentiated cells suitable for transplantation. For this purpose, two main reprogramming approaches are currently available. One reprograms somatic cells into induced pluripotent stem cells (iPSCs) by the induction of the four Yamanaka factors[1,2,3] and subsequently differentiates them into the desired somatic cells. The other is transdifferentiation, which is the direct conversion of one somatic cell type to another without going through pluripotency, by the manipulation of one or more ectopic master regulator transcription factors[4,5]. Both of these reprogramming approaches face critical challenges of producing optimized cultures of reprogrammed target cells with high level of efficiency and quality. In order to meet these challenges a fully controlled directed differentiation and transdifferentiation is needed.

To date numerous studies have manipulated stem cell differentiation and cell fate redirection by cell culture growth media and microenvironment conditions[6]. However,

it remains to be known whether pluripotent stem cells (ESCs or iPSCs) would be directly differentiated by inducing expression of a lineage specific master regulator that is known to successfully redirect cell fate in somatic cells

ESCs are pluripotent cells derived from the inner cell mass of blastocyst-stage embryos that have the capacity to give rise to differentiated derivatives from all three primary germ layers: ectoderm, mesoderm, and endoderm[7]. iPSCs share chromatin structure and gene expression characteristics with ESCs[8]. ESCs differentiation into specialized cells requires the use of differentiation media that contains specific growth and signaling factors per se or in combination with the expression of defined transcription factors [6]. This approach has been used to differentiate ESCs into melanocytes[9,10,11].

Microphthalmia-associated transcription factor (MITF) is a basic helix–loop–helix (bHLH-zip) transcription factor that serves as the master regulator of the melanocyte lineage. Nonfunctional MITF results in lack of melanocytes[12,13]. Alternative promoters give rise to various MITF isoforms differing in their N-termini; promoter use is regulated in a tissue-specific manner[14]. The promoters of genes regulated by the melanocyte specific isoform, M-*MITF*, contain the consensus E-box sequence[12]. MITF regulates the transcription of melanocyte-specific genes: *TRPM1*, *TYR*, *TYRP1*, *DCT*, *SILV*, and *MLANA* as well as genes involved in cell survival and proliferation such as *BCL2*, *CDK2*, and *DICER*[15]. MITF has a critical role in melanoma as it is required for survival and controls the proliferative, invasive, and metastatic properties of melanoma cells[16,17].

It was previously reported that ectopic expression of *Mitf* converts fibroblasts into cells with melanocyte characteristics, although only a minority of the *Mitf*-transfected cells had a melanocyte-like cell appearance[18]. A recent study showed that about 10% of the fibroblasts infected with retroviruses carrying a combination of transcription factors MITF, SOX10, and PAX3 acquire melanocyte properties[19].

In an effort to produce highly efficient, directed differentiation and transdifferentiation systems, we have analyzed effects of inducible expression of the MITF master regulator in differentiation promoting growth conditions in both somatic cells and pluripotent ESCs. We developed a transgenic system in which *Mitf* expression was Dox-inducible that enabled us to screen MITF reprogramming potential on different primary cell types

originating from the same animal model and also to direct differentiation of pluripotent mouse ESCs (mESCs).

Results

Generation of doxycycline-inducible *Mitf* knock-in reprogrammable system

In order to test the potential of different cell types to switch lineage in response to a single lineage master regulator expression, we established a Dox-inducible mouse model using the melanocyte lineage specific isoform of *Mitf* (M-*Mitf*). M-*Mitf* serves here as an exclusive inducer of differentiation and transdifferentiation unlike the conventional method based on media promoting factors. We used KH2 mESCs that constitutively express the M2 reverse tetracycline transactivator (M2rtTA)[20] from the *ROSA26* locus (*ROSA26*-M2rtTA). A Dox-responsive element controlling *Mitf* expression was targeted downstream of the *collagen 1a1* locus by frt/Flpase-mediated site-specific integration (*Col1a1-TetO-Mitf*). In order to visualize the engineered mESCs, pBRY-CAGGS-mCherry encoding transgene was transduced into the correctly targeted mESCs (Fig. 1a, b). mESCs were injected into host E3.5 mouse blastocysts and chimeric embryos were dissected at 13.5E and were used to generate mouse embryonic fibroblast cultures (MEFs). Chimeric newborn P1-3 mice were also generated and somatic tissues were analyzed (Fig. 1c). The constitutively expressed *mCherry* allele and puromycin resistance cassettes allowed us to easily isolate and purify the *Mitf* transgenic cells from chimeric cultures and animals.

Highly efficient transdifferentiation of MEFs into melanocyte-like cells by MITF

Somatic cell transdifferentiation into melanocyte-like cells has been previously reported in MEFs at efficiencies of 2% to 10% [18, 19]. Although transdifferentiation is considered to be superior in terms of reprogramming efficiency as compared to conventional iPSCs reprogramming, the acceptable range of transdifferentiation protocols is up to 20% efficiency of the source cell population[21,22,23].

We first aimed to validate the ability of Dox-induced *Mitf* expression to stimulate transdifferentiation in mouse cells. We generated MEFs from the engineered mouse chimera embryos and induced *Mitf* expression by supplementing growth media with

Dox. Dox-treated *Mitf* knock-in MEFs acquired a dendrite like morphology that is a distinctive characteristic of melanocytes[24] (Fig. 2a) whereas *Mitf* knock-in mESCs appearance remained unchanged (Supplementary Fig. 1a).

We then examined expression of known MITF target genes upon Dox induction. *Mitf* knock-in MEFs showed higher expression of melanogenic markers at 6 days post Dox induction than at earlier time points (Supplementary Fig. 1b, c). We therefore treated *Mitf* knock-in MEF and mESCs cells for 6 days and demonstrated upregulation of MITF target genes, TYRP1 and TYR (Fig. 2b and Supplementary Fig. 1d). Moreover, TYRP1 upregulation in Dox-treated MEFs compared to the vehicle-treated MEFs was demonstrated by immunostaining (Fig. 2c) and quantified (Supplementary Fig. 1e, f). MITF, as an expected of a transcription factor, was localized to the nucleus, whereas TYRP1 was found in the cytoplasm since it is part of the secreted pigment-producing vesicles [25] that are trafficked from melanocytes to adjacent cells [26]. Finally, to examine the global effect on the transcriptome, we performed a global mRNA expression profiling via RNA-seq. Genes differentially expressed in *Mitf* knock-in MEFs compared to vehicle-treated knock-in MEFs (Supplementary Tables 1 and 2) were clustered and compared to expression in untreated wild-type MEFs and primary mouse melanocytes (PMel) (Fig. 2d). This clustering demonstrates a gradual transition in the expression profile of Dox-treated *Mitf* knock-in MEFs toward the melanocyte expression profile (Fig. 2d). Likewise, Spearman correlation coefficients clearly demonstrate that Dox-treated *Mitf* knock-in MEFs (Dox+) are more similar to primary melanocytes (0.26) than to untreated *Mitf* knock-in MEFs (0.048), but overall Dox-treated knock-in MEFs are still more similar to wild-type MEFs (0.73) than to primary melanocytes (Fig. 2e). Indicating that Dox+ are MEFs that started to change upon primary melanocytes, but on the imaginary differentiation trajectory it are still closer to untreated MEFs. In summary, the *Mitf* inducible transgenic system recapitulated the previously reported transdifferentiation ability of MITF in mouse fibroblasts [27]. The higher efficiency is likely attributed to an optimized transgenic delivery of the reprogramming factor and to higher levels of factor induction than obtained during heterogeneous primary transduction with viruses [28].

OCT4 impedes differentiation in mESCs despite MITF expression

Successful transdifferentiation by MITF in somatic cells encouraged us to further investigate our hypothesis in ESCs. Since naïve ESCs are pluripotent and their euchromatin to heterochromatin ratio is higher than in somatic cells [29], we reasoned that ESCs might be favorable for manipulations, thereby enabling directed differentiation by MITF induction. In order to test this assumption, in addition to *Mitf* knock-in mESCs and *Mitf* knock-in MEFs, we also generated primary cell cultures from the intestine, heart, and brain of *Mitf* knock-in mouse chimeric newborns as these tissues represent the three germ layers endoderm, mesoderm, and ectoderm, respectively (Fig. 3a). We validated the quality of cell isolation by measuring expression of lineage specific markers (Fig. 3b). This analysis indicated high purity of isolation for each tissue. Next, *Mitf* expression was induced in all of the indicated preparations by addition of Dox to the growth media for 6 days. Interestingly, *Mitf* was upregulated in all cell types, however, MITF target genes were not upregulated in mESCs, although these genes were upregulated in other tested somatic cell types (Fig. 3c).

In order to elucidate why mESCs were less responsive to *Mitf* induction, we profiled gene expression using the "BioGPS" gene annotation portal (Supplementary Table 3). Our first speculation was that mESCs, unlike the other cells, lack the expression of melanocyte lineage developmental genes such as *Ednrb*, *Edn3*, *Sox10*, and *Pax3* [13]; however, all of the investigated cells exhibited comparable expression amounts of melanocyte lineage developmental genes (Fig. 3d). This suggested that there are factors that prevent mESCs differentiation upon *Mitf* induction.

Possible candidates are OCT4, SOX2, and NANOGg, which are the core factors that maintain the pluripotent state and which play vital roles in the control of specific cell fates dependent on their defined levels [30,31 ,32]. In order to investigate whether one or more of these factors block MITF from upregulating its target genes, we first overexpressed *OCT4*, *SOX2*, or *NANOG* in MEFs followed by *Mitf* induction. Interestingly, although *Mitf* was significantly induced, there was only minor upregulation of its specific target genes *Tyrp1*, *Trpm1*, and *Tyrosinase* when *OCT4* was overexpressed (Fig. 3e). *SOX2* overexpression blocked *Trpm1* upregulation but not induction of *Tyrp1* and *Tyrosinase*, suggesting a more dominant role for *OCT4*. *OCT4* overexpression (confirmed as shown in Supplementary Fig. 2) in Dox-treated *Mitf*

knock in MEFs also inhibited TYR activity (Fig. 3f) as shown using a florescent dye bound to the tyrosine analog tyramide, which is a substrate for TYR [33]. In a reciprocal experiment, we inhibited expression of *Oct4*, using validated shRNA compared to sh-control, followed by *Mitf* induction in *Mitf*-inducible mESCs. Samples showed that *Mitf* upregulates its target genes *Tyrp2*, *Trpm1*, and *Tyrosinase* in mESCs deficient in *Oct4* (Fig. 3g).

In summary, the above data indicate that OCT4 impedes MITF activity in mESCs and in somatic cells upon ectopic expression of OCT4. This suggests that OCT4 protects against destabilization pluripotency potential, by blocking MITF pro-differentiation activity. We therefore reasoned that for a highly efficient directed differentiation of mESCs by *Mitf* induction, similarly to *Mitf* induced transdifferentiation of MEFs, a concomitant *Oct4* suppression is required in order to release the stem cells from pluripotency.

OCT4 interferes with MITF transcriptional activity

To explore the mechanism underlying OCT4 interference with the pro-differentiation activity of MITF, we examined OCT4 and MITF genomic occupancy by analysis of ChIP-seq data of MITF in human melanocytes[34] and OCT4 in human ESCs [35]. We found that 26% of promoters bound by MITF were also bound by OCT4, and in 13% of these regions OCT4 bound within 10 Kb of the MITF-bound region (Fig. 4a). Of regions bound by MITF, 39% were also bound by OCT4 in a close proximity of less than 3Kb (Fig. 4b). For instance, regions upstream of *TRPM1* and *TYR*, genes strongly related to melanocyte identity, were occupied by both MITF and OCT4 (Fig. 4c). Moreover, *TRPM1* and *TYR* promoter regions contained not only the well-documented MITF binding consensus site (the E-box) [12] but also the known OCT4 binding motif [36] (Fig. 4c).

Next, we tested the capability of OCT4 to influence MITF transcriptional activity by using reporter constructs in which luciferase expression was driven by the *TRPM1* or *TYR* promoter. We compared effects of wild-type OCT4 to that of a mutated OCT4 which was phosphorylated in a site located within the OCT4 homeobox domain (T234 and S235) and found to negatively regulate OCT4 by disrupting sequence-specific DNA binding [37]. TRPM1 or TYR reporter was co-transfected with an MITF expression

vector and wild-type or mutant OCT4 expression plasmid. Cells with high MITF levels, were co-transfected with TRPM1 or TYR reporters and wild-type or mutant OCT4 expression vector. In both systems, wild-type OCT4 significantly decreased MITF transcriptional activation of TRPM1 and TYR whereas mutant OCT4 did not (Fig. 4d). OCT4 also inhibited MITF-induced transcription of mouse MLANA reporter (Supplementary Fig. 3a). SOX2 and NANOG overexpression in these systems did not inhibit expression from the reporters as OCT4 did (Supplementary Fig. 3b). When melanoma cells with high MITF levels were transfected with a vector for expression of OCT4 there was a reduction of both *TRPM1* and *TYR* expression (Fig. 4e). Furthermore, melanoma cells with low MITF levels that were transfected with vectors for expression of MITF and OCT4 showed a significant decrease in *TRPM1* mRNA levels compared to the control (Fig. 4e). Interestingly, *OCT4* and *MITF* are inversely correlated in different melanoma cell lines (Supplementary Fig. 4a) and seem to be uniquely expressed in skin cutaneous melanoma (Supplementary Fig. 4b).

To further study the OCT4 mechanism of action in regulating MITF transcriptional activity, co - immunoprecipitation experiments were performed to test their physical interaction. Cells were transfected with vectors for expression of MITF-HA and OCT4-Flag, and HA antibody was used for immunoprecipitation. In addition, cells that endogenously express MITF were transfected with OCT4-Flag, and immunoprecipitation was done using antibody against MITF. These experiments demonstrated that OCT4 and MITF physically interact (Fig. 4f; Supplementary Fig. 3c). To confirm that there is a functional interaction between OCT4 and MITF, electrophoretic mobility shift assay (EMSA) experiments were conducted that demonstrated that MITF binding to the E-box consensus site in the *TRPM1* promoter was blocked by OCT4 (Fig. 4g; Supplementary Fig. 3d). Taken together, our data indicate that OCT4 interrupts MITF-mediated transcriptional activity by preventing MITF binding to the promoter region of its putative target genes.

Oct4 maintains pluripotency and prevents differentiation

Next, we aimed to explore whether OCT4 interference with MITF transcriptional activity is a global phenomenon and whether other somatic lineage commitment transcription factors are subjected to such regulation. Therefore, we analyzed ChIP-seq data of OCT4 and the following lineage transcription factors: MITF [34], CDX2, GATA4

[38], and HES1 [39], which are central in the differentiation of melanocytes, intestinal cells, cardiac cells, and astrocytes, respectively (Fig. 5a). There was significant overlap of genes bound by OCT4 and these transcription factors (-log10 P-values for the overlap between OCT4 and MITF, 222.53; HES1, 177.38; GATA4, 235.73; CDX2, 193.11). Using the DAVID functional annotation tool, we performed a Gene Ontology (GO) enrichment analysis of the co-bound genes (Supplementary Table 4). Significance of the obtained biological pathways was determined according to Benjamini-Hochberg multiple testing rate. The pathways that were considered significant scored below 0.05 in this parameter. The identified biological pathways clearly showed that OCT4 occupies promoters of genes that are essential for specific lineage development (Fig. 5b). For example, GO analysis of genes co-bound by OCT4 and MITF revealed significant enrichment of the melanin pigmentation process, which uniquely characterizes melanocytes and is also known to be regulated by MITF [40]. Similarly, analysis of OCT4 and GATA4 bound genes revealed significant enrichment in genes involved in cardiac development, which is known to be regulated by GATA4 [41, 42]. Importantly, the non-overlapping genes yielded only general biological pathways and not genes known to be regulated by the lineage-specific transcription factors (Supplementary Table 5).

In order to explore whether OCT4 uniquely occupies promoters of genes involved in developmental lineage pathways, we analyzed ChIP-seq data of the general transcription factor E2F7 for overlap with MITF-bound genes. In the GO analysis of co-bound genes we found no significant enrichment in developmental pathways (Supplementary Table 6; Supplementary Fig. 5a, b). Additional analyses of MITF ChIP-seq data generated in normal melanocytes [43] with ChIP-seq peaks of OCT4, E2F7, or P53, followed by GO analysis of overlapping genes (Supplementary Table 6) showed that only MITF and OCT4 co-bound genes resulted in significant melanocyte differentiation pathway enrichment (Supplementary Fig. 5). No enrichment in genes involved in differentiation was observed in the genes bound by MITF and E2F7 or P53. No other classes of genes were significantly enriched in these overlapping targets.

These data suggest that OCT4 occupies lineage-specific gene promoters in order to prevent transcriptional activity under inappropriate timing. To test this hypothesis *in vivo*, we used mice in which *Oct4* expression was inducible[44]. We derived transgenic

melanocytes and cell cultures from the brain, heart, and intestine of newborns (Fig. 5c). The expression of cell type specific markers was significantly decreased following *Oct4* induction (Fig. 5d).

We also examined OCT4 in relation to other transcription factors in another regulatory layer of chromosome organization. The Hi-C method was developed to enable exploration of genome-wide chromosomal associations[45]. Segments of internal high spatial connectivity termed "topologically associating domains" (TADs)[46,47]. Clustering of genes that in TADs are co-regulated in nuclear sub-compartments, which comprise the contact domains, may facilitate their co-regulation by favoring frequent engagement with enhancers within TADs while insulating the influence of the enhancers beyond the TAD borders create nuclear microenvironments that are enriched in specific factors that coordinate the expression or repression of specific groups of genes[48,49]. Since TAD borders are stable acress different cell types[50], we integrated Hi-C data of human lymphoblastoid cells together with ChIP-seq data. This analysis showed a significant sharing domain binding between OCT4 and a number of transcription factors in TADs (Fig. 5e). Assuming that the loci bound by transcription factors are connected in three dimensions to genes within the same TAD, the enrichment of particular transcription factors in the same TAD suggests that they co-regulate genes found in the TAD. To visually demonstrate our analysis, we used "Juicebox" software for visualizing data from Hi-C mapping experiments. By this analysis, for example, the MITF target gene TRPM1 was found to be in an OCT4 and MITF shared TAD (Fig. 5f), supporting our hypothesis that OCT4 interferes with MITF transcriptional activity by sharing the same TADs (Supplementary Table 7). These findings indicate that cell type-specific regulatory sites can be engaged by a combination of transcription factors in a cooperative manner.

Finally, we analyzed the enhancers occupied by MITF and determined whether OCT4 or P53 co-bind these regions (Supplementary Table 8). We counted the number of MITF, OCT4, and P53 ChIP-seq peaks within ESCs enhancers. We found that 1.6% of enhancers are bound by MITF and 11% of MITF-bound enhancers are also bound by OCT4 (-log(p-value=122)). In contrast, only 0.57% of MITF-bound enhancers are also bound by *P53* (-log(p-value=5)) (Fig. 5g). This result implies that the regulatory interaction between MITF and OCT4 occurs in both enhancers and promotors. This

strengthens our hypothesis that there is a transcriptional regulatory competition between MITF and OCT4.

Discussion

Transdifferentiation of somatic cells can be achieved by the expression of a specific set of transcription factors. It has been reported that the expression of MITF alone or in combination with other transcription factors can induce transdifferentiation of fibroblasts into cells with melanocyte characteristics[18,19]. In this study, we first showed that MEFs can be induced to transition into melanocyte-like cells with high efficiency using an optimized Dox-dependent *Mitf* knock-in system. We also demonstrated that MITF was able to transdifferentiate the investigated somatic cells. Our findings confirm the role of MITF as a master regulator of melanocytes, reminiscent of the master role of MyoD in inducing fibroblast transdifferentiation into muscle[51].

To date, most protocols designed to induce changes in cell fate have focused on reprogramming of a specific cell type[4,5] and these protocols have not been systemically characterized[51]. Here we evaluated a repertoire of primary somatic and embryonic stem cells that originated from the same mouse model and subjected them to the induction of a master differentiation and transdifferentiation regulator, MITF. In contrast to previous reports of transdifferentiation in which indicated that effects of expression of a master regulator were limited to target cells closely related to the originating cells[4], we observed highly efficient induction of transdifferentiation that was not restricted to a specific cell type. We demonstrated transdifferentiation of cells from all three germ layers, however, mESCs did not exhibit a transition into melanocyte-like cells upon *Mitf* induction.

Since ESCs possess a more open chromatin configuration than somatic cells and thus have higher developmental plasticity, we expected that ESCs would be more susceptible to transcription factor occupancy than somatic cells. Interestingly, although *Mitf* was induced at high levels in ESCs, it did not promote efficient differentiation into melanocytes. In order to identify the factor responsible for blocking MITF-induced differentiation of ESCs, we focused on the pluripotent master regulators OCT4, SOX2, and NANOG since all are well established to control pluripotent cell fate decisions[30,31,32]. This suggests that OCT4 may inhibit the induction of differentiation by MITF in

pluripotent cells by physical interaction with MITF, thus interfering MITF from regulating its target genes.

The role of OCT4 in reprogramming of somatic cells into pluripotent stem cells has been widely studied [52]. Recently, Chronis et al. showed that an important step in this process requires the silencing of MEFs enhancers and promoters by OCT4, SOX2, KLF4, and cMYC. Interestingly, these transcription factors induce the relocation of somatic transcription factors from the MEF enhancers, emphasizing their role in blocking somatic transcription factor-dependent differentiation[53]. Computational analysis demonstrated that OCT4 occupies the promoter and enhancer regions of MITF target genes in melanoma cells and melanocytes and also shares chromatin contact domains with MITF. In contrast, there were no lineage-related pathways were enriched in GO analyses of genes that bound MITF and general transcription factors E2F7 or P53. SOX2 and NANOG also appear to compete for binding to gene promoters with lineage-specific transcription factors in a similar manner as OCT4 as demonstrated by significant GO enrichment for lineage pathways (Supplementary Tables 9 and 10). Interestingly, when comparing OCT4 [35], SOX2, and NANOG promoter occupancies [54], OCT4 and NANOG together seem to engage more gene promoters than combinations of OCT4 and SOX2 or SOX2 and NANOG (Supplementary Fig. 6). OCT4 also occupies gene promoter regions and topological domains of somatic lineage transcription factor target genes as well.

Taken together our observations strongly suggest that the ability of MITF to differentiate pluripotent mESCs is tempered by OCT4 interference (Supplementary Fig. 7) at the transcriptional level. That expression of MITF, which serves as a model for other lineage master regulators, efficiently switched cell fate of inter germ layers opens new opportunities in the field of regenerative medicine. It will be of interest to validate a role for OCT4 in human somatic cell reprogramming as well.

Methods

Mice

Dox inducible *Oct4* mice: The Oct-4/rtTA (ROSA26-M2rtTA;Col1a1-tetO-Oct4) mice were purchased from the Jackson Laboratory (JAX Stock# 006911).

Dox inducible *Mitf* mice: To enable efficient generation of targeted ESCs harboring a single Dox-regulated *Mitf* gene, we adapted the ColA1 Flp/FRT recombinase-mediated targeting system previously described by Jaenisch and colleagues [55]. Specifically, we have used mouse melanocyte specific isoform, M-*Mitf*, flanked by flippase recognition target (FRT) sites. Pre-engineered 'KH2' ESCs contain a FRT-hygro-pA "homing" cassette downstream of the *ColA1* gene (CHC), as well as a reverse tet-transactivator (rtTA) targeted to the *ROSA26* locus (R26-rtTA). Following co-electroporation of pCAGs-Flpe and an appropriate targeting vector, Flpe-mediated recombination between the FRT site at the ColA1 locus and those present on the targeting vector confers hygromycin resistance only if correctly integrated [55]. The resulted mESCs were called *Rosa26* RtTa, *Col1a Mitf*. In order to validate M-*Mitf* insertion, mESCs were subjected to restriction enzyme (SpeI) treatment followed by DNA extraction and southern blot. M-*Mitf* in ColA1 locus represented by a 4.1 KB fragment compared to 6.2 KB fragment in the wild type mESCs (Figure 2b). In order to create MEFs carrying Dox inducible *Mitf*, engineered mESCs were microinjected into the inner cell mass (ICM) of BDF2 blastocysts that were implanted into pseudo pregnant female mice. E13.5 or adult chimeric embryos/mice were used to isolate somatic cells.

Tissue culture

For generation of MEFs, 13.5E embryos were freshly isolated and their body was enzymatically and mechanically dissociated. WM3314 and WM3682 melanoma cells were kindly given by Dr. Levi A. Garraway (Department of Medical Oncology and Center for Cancer Genome Discovery, Dana-Farber Cancer Institute, Boston, MA). Cells were cultured in DMEM medium supplemented with 10% fetal bovine serum (FBS) (Sigma-Aldrich), 2 mM l-glutamine and 1% penicillin/streptomycin/glutamine (Invitrogen). For generation of mouse embryonic stem cells (mESCs), E3.5 blastocysts were collected and the ICM were dissected mechanically. The cells were plated on irradiated feeder layers (e.g. MEFs) seeded on gelatin-coated 6-well plates and kept in

ESCs medium [DMEM with 20% FBS (Invitrogen), 1× nonessential amino acids, 2 mM l-glutamine, 0.1 mM β-meraptoethanol and 1000 IU/ml leukemia inhibitory factor (LIF)]. After approximately 4–5 days, the outgrowths were trypsinized and dissociated into small cell masses and single cells. These cells were plated on fresh feeders to generate established ES lines.

RNA Purification and qRT-PCR

Total RNA was purified using Trizol (Invitrogen) according to manufacturer's instructions followed by treatment with RNase-free DNase (QIAGEN). RNA was quantified by measuring OD260/280. For mRNAs analysis, RNA was subjected to one-step qRT-PCR using a MultiScribe RT-PCR kit (Applied Biosystems) and FastStart Universal SYBR Green Master (Rox) (Roche). All experiments are $n \geq 3$. Standard error of the mean (SEM) is presented. All qPCR primers are listed in Supplementary Table 12.

Plasmids and cloning

hOCT3/4-Flag, hSOX2-Flag and hNANOG-Flag expression vectors were obtained through Addgene. MITF-HA expression vector and pGL3b-hTRPM1-luciferase were kindly obtained from Dr. David. E. Fisher (Department of Dermatology, Cutaneous Biology Research Center, Massachusetts General Hospital, Harvard Medical School, MA). pCEP4_WT_OCT4 and pCEP4_OCT4_T234E_S235E expression vectors were obtained through Addgene.

Virus preparation and transduction

Lentiviral Particles harboring shRNA of mouse *Oct3/4*, *Sox2*, *Nanog* and Control shRNA Lentiviral Particles were purchased from Santa Cruz Biotechnology. MLV particles used for *Oct4* and *Sox2* overexpression were generated using the pCL-Eco packaging plasmid and pMXs-hOCT3/4 or pMXs-hSOX2 (Addgene through Dr. Jacob Hanna). Both plasmids were co-transfected to HEK293T cells using jetPEI™. 24h later, viruses were filtered and frozen in -80°C. Viruses were transduced to mESCs or MEFs using Polybrene ® (Santa Cruz) in final concentration of 1µg/ml. 24h later supernatant was replaced to a fresh growth media.

Southern blot

Genomic DNA was extracted from each hygromycin-resistant targeted subclone. 10–15 μg of genomic DNA was digested with SpeI restriction enzyme for 5 h and separated by gel electrophoresis. The DNA was transferred to a nitrocellulose membrane that was next hybridized with a radioactively labeled probe and developed using enhanced chemiluminescent substrate (Thermo Scientific).

Engineered primary somatic cell generation

Newborn were used at day 1-3. Melanocytes were extracted from the epidermis. Skin was removed into 0.25% trypsin and incubated overnight at 4ºC. Next, dermis and epidermis were separated. Epidermis was incubated at 37°C in 0.25% trypsin for 30 minutes and then dispersed into small pieces and covered with melanocyte media. The cells were not touched until day 4 post extraction. Cells from the brain were obtained based on Saura et al [56]. Cells from heart and intestine were isolated based on Song et al [57] . Shortly, heart and intestine were dispersed by addition of 0.625 mg/ml collagenase (type II; Worthington) and incubated at 37ºC for 40 min. Cells were resuspended with fresh DMEM with 10% FCS and centrifuged at 1000 rpm for 3 min. Cell pellet was suspended in DMEM with 10% FCS. Cells originated from the heart were plated on gelatin coated plates.

Transfection and luciferase reporter assay

Luciferase reporter driven constructs were co-transfected with the pcDNA3-MITF-HA or empty plasmid into HEK293T cells or WM3682 in 24-well plates (total of 1 µg DNA/well) using jetPEI™ for HEK293T or *Trans*IT-X2® for WM3682 according to the manufacturer's instructions. Cell lysates were prepared 48h after transfection, followed by activity measurement of FireFly luciferase, using the Dual Luciferase kit (Promega) according to the manufacturer's recommendations. Promoter activity was normalized to the constitutively expressed Renilla or to protein quantity as measured by Bradford reagent. For MEFs transfection *Trans*IT-X2® reagent was used.

Gel electrophoresis and immunoblotting

Melanoma cells were lysed 48hr after transfection and MEFs were lysed at day 6 and 12 post Dox induction in buffer containing 50 mM Tris (pH 7.4), 150 mM NaCl, 1% Triton X-100 and protease inhibitor cocktail (Sigma-Aldrich). Samples (40µg) were resolved by 10% SDS-PAGE, transferred to nitrocellulose membranes, and exposed to the appropriate antibodies: rat monoclonal HA-probe antibody (Roche) or mouse monoclonal ANTI-FLAG®M2 antibody (Sigma-Aldrich) or rabbit anti-TYRP1 (a gift from the Vincent Hearing lab, NCI) or mouse monoclonal C5 anti MITF, kindly provided by Dr. David. E. Fisher (Department of Dermatology, Cutaneous Biology Research Center, Massachusetts General Hospital, Harvard Medical School, MA). Proteins were visualized with SuperSignal Chemiluminescent Substrates (Pierce), using horseradish peroxidase-conjugated anti-mouse secondary antibody (7076; Cell Signaling). Western blot assays shown are representative of at least three experiments.

Immunostaining

MEFs were cultured on glass cover slips (13 mm, 1.5 H; Marienfeld, 0117530), washed three times with PBS and fixated with 4% paraformaldehyde for 10 min at room temperature. Cells were then permeabilized and blocked in 0.1% Triton, 0.1% Tween and 5% FBS in PBS for 15 min at room temperature. Primary antibodies were incubated for 2 h at room temperature and then washed with 0.1% Tween and 1% FBS in PBS three times. Next, cells were incubated with secondary antibody for 1 h at room temperature, washed and counterstained with DAPI, mounted with Shandon Immu-

Mount (Thermo Scientific) and imaged. All secondary antibodies were diluted 1:200. The following antibodies were used: rabbit anti MITF antibody (a gift from the David E Fisher lab, DF/HCC). rabbit anti-TYRP1 (a gift from the Vincent Hearing lab, NCI). Mouse monoclonal ANTI-FLAG®M2 antibody (Sigma-Aldrich).

Co-Immunopercipitation (Co-IP)

pcDNA3-MITF-HA and pcDNA3-OCT4-Flag were transfected individually or together into HEK293T cells in 10cm culture plate (total of 10 µg DNA/well). WM3682 cells were transfected with pcDNA3-OCT4-Flag. Cell lysates were prepared 48h after transfection using IP buffer containing protease inhibitor cocktail (Sigma-Aldrich). Samples were incubated with rat monoclonal HA-probe antibody (Roche) primary antibody (for HEK293T) or rabbit anti MITF antibody (a gift from the David E Fisher lab, DF/HCC) (for WM3682) overnight at 4ºC. Antibody-antigen complexes were precipitated by incubation of the sample with 30µl Protein A/G PLUS-Agarose beads (Santa Cruz) for 2h at 4ºC. Beads were washed 5 times with IP buffer. Then boiled at 95ºC for 5min X2 with loading buffer. The Immunoprecipitated material was subsequently investigated by western blot analysis using primary antibodies: rat monoclonal HA-probe antibody (Roche) or mouse monoclonal ANTI-FLAG®M2 antibody (Sigma-Aldrich). Proteins were visualized with SuperSignal Chemiluminescent Substrates (Pierce), using horseradish peroxidase-conjugated anti-mouse secondary antibody (7076; Cell Signaling).

Electrophoretic mobility shift assay (EMSA)

Nuclear extracts were prepared using a NE-PER nuclear and cytoplasmic extraction kit (Pierce) according to the manufacturer's instructions. The *MITF* biotin-labeled DNA probes spanning *MITF* binding sites were obtained from IDT. Binding reactions of 10 µg of nuclear lysates and 0.02 pmol of labeled double-stranded DNA probe were performed for 20 min on ice using a LightShift chemiluminescent EMSA kit (Pierce) according to the manufacturer's instructions. Competition analyses were performed with an excess (30 pmol) of unlabeled probes. Samples were resolved by 5% PAGE in 0.5× TBE buffer (45 mM Tris borate, 1 mM EDTA) transferred to nylon membranes. Labeled DNA was visualized with the ECL system (Pierce). The super-shift assay is shown in Supplementary Figure 6. Probe sequence for the *MITF* binding site is listed

in Supplementary Table 12. The wild-type probe was derived from the *TRPM1* promoter, which was shown to bind *MITF* [58].

Tyramide-Based Tyrosinase Activity Assay

The assay was performed according to[59]. Briefly, confluent MEF cell cultures were scraped and washed three times with phosphate-buffered saline (PBS), pH 7.4. Smears of the final cell suspensions were air-dried and tested. Air-dried smears were permeabilized in 0.1% Triton X-100 in PBS for 5 min at room temperature. Tyramide-Cy5 was reconstituted in 50 µL of dimethyl sulfoxide (DMSO), according to the manufacturer's specifications, diluted in 250 µL of Tyramide Signal Amplification (TSA) diluent (Perkin Elmer Life Science Products, Boston, MA), and applied (50 µL/each) to the slides containing permeabilized cells. The slides were then incubated in a humid chamber at room temperature for 20 min, followed by three washes (X3) with PBS and water (X1). Image analysis of the cells was performed on Leica TCS STED (Stimulated Emission Depletion) confocal microscope. Pixels of 10 nuclei were quantified using the Image J software.

Microscopy and image analysis

Images were acquired with A1 Axioscope microscope (Carl Zeiss) equipped with DP73 camera (Olympus) or with Z1 Axioscope microscope (Carl Zeiss), Fluorescent images were quantitatively analyzed using ImageJ software.

Enrichment of OCT4 and lineage TFs in Hi-C domains:

Genomic topologically associating domains (TADs) in GM12878, as defined by Rao et al. 2014 [60], were used for this analysis. Overlapping domains were removed keeping the shortest domains of each region. ChIP-seq data for each TF[61] was used to assign TF binding in each domain. To test for enrichment of both TF peaks within domains we used two methods: 1) Hypergeometric distribution test: hypergeometric score was defined in order to examine the enrichment of OCT4 peaks and a second TF peaks within Hi-C domains. 2) Permutation test: The peaks of the two TFs were shuffled between the domains, keeping the original distribution of the number of peaks in different domain lengths. This was done by grouping the domains by their length and

shuffling the number of TF peaks between each group. This was done 10,000 times, each time calculating the number of domains containing both TFs peaks.

RNA sequencing and gene expression profiling analysis

RNA was extracted from Trizol pellets of wild type MEFs, Dox treated *Mitf* knock-in MEFs for 6 days, untreated *Mitf* knock-in MEFs and primary mouse melanocytes, and utilized for RNA-seq by TruSeq RNA Sample Preparation Kit v2 (*Illumina*) according to manufacturer's instruction. DNA sequencing was conducted on Illumina Hiseq1500. Tophat software version 2.0.10 was used to align reads to mouse mm10 reference genome (*UCSC, December 2011*). Read counts per exon were calculated over all 628,052 exons in mm10 ensemble GTF (*UCSC, December 2011*), using bedtools coverage command (version 2.16.2). Exons annotated as protein coding, pseudogene or lincRNA (n=459,556) were selected for further analysis. Exon counts were normalized by the exon length in Kbp and by million number of aligned reads per sample, to give RPKM values. Only exons with at least one RPKM call > 10 were selected, resulting in 163,841 exons corresponding to 14,980 genes. Furthermore, exons were filtered to include only exons that show abs(FC)>4 between MEF and Melanocyte, resulting in 45,155 differentially expressed exons corresponding to 5,864 genes. Spearman correlation between samples were done using Matlab (version R2016b) over all exons (Fig 2.e). Gene expression was defined by the maximal expression level (RPKM) of all exons associated to a certain gene. Hierarchical clustering was calculated over all differential genes (5,864 genes) Matlab (version R2016b) clustergram command, using Spearman correlation as a distance metric, ward linkage, and per-row standardization (zscore) (Fig 2.d).

Promoter and Enhancer analysis

ChIP-seq peaks of each transcription factor were collected from the ENCODE project consortium[61] and assigned to promoters (using different transcription start site (TSS) distances to define promoters) and enhancers (using human embryonic stem cells enhancers as defined by Ernst et al[62] and appears at ENCODE (http://hgdownload.cse.ucsc.edu/goldenPath/hg19/encodeDCC/wgEncodeBroadHmm/). To test for enrichment of two TFs within promoters or enhancers we used

Hypergoemtric distribution test. We further explored the distance of *OCT4* peaks from promoter/enhancer-*MITF* peaks up to 10kb.

Figure Legends

Figure 1: Generation of doxycycline-inducible *Mitf* knock-in reprogrammable system. (a) A schematic illustration of the Frt-tetO-*Mitf* knock-in construct directed to the Flpe mCol1a cassette. Also indicated are 3' Southern blot external probes and the nuclear mCherry transgene marker. (b) Southern blot verification of tetO-*Mitf* knock-in to ESCs. Clone #3 was incorrectly targeted, whereas clone #4 was correctly targeted and was used for injection into E3.5blastocyst to obtain ROSA26-M2RtTa$^{+/+}$mCol1a-TetO-*Mitf*$^{+/-}$ derived MEFS and somatic cells. (c) A schematic illustration of the *Mitf* knock-in reprogrammable MEFs and somatic cells.

Figure 2: Highly efficient transdifferentiation of MEFs into melanocyte-like cells by MITF. (a) Bright field images of *Mitf* knock-in MEFs showing morphological changes at 12 days after *Mitf* induction by Dox supplemention and of untreated *Mitf* knock-in MEFs and primary mouse melanocytes. (b) MITF and TYRP1 protein levels in *Mitf* knock-in MEFs at days 6 and 12 post Dox induction. (c) Immunostaining of MITF (green) and TYRP1 (purple) in MEFs at day 6 post Dox induction with endogenous expression of mCherry (red). (d) Hierarchical clustering of genes differentially expressed in MEFs before and after induction of *Mitf* expression (5,864 genes) using Spearman correlation as a distance metric, Ward's linkage, and per-row standardization (z score). (e) Spearman's correlation was calculated over all exons that show differential (>4 fold change) expression between MEFs and melanocyte samples (45,155 exons).

Figure 3: OCT4 impedes differentiation in mESCs despite *Mitf* expression. (a) Representative microscopy images of mESCs, MEFs, and cells from the intestine, heart, and brain from *Mitf* knock-in chimera mice. (b) Expression of lineage specific markers in the investigated cell types are shown. Levels were normalized to *Gapdh*. Error bars represent ± SEM(n = 3). (c) *Mitf*, *Tyrp1*, *Tyrp2*, *Trpm1*, and *Tyrosinase* mRNA levels in the indicated cells at day 6 post Dox induction and in vehicle-treated cells. Relative levels were normalized to *Gapdh*. Error bars represent ± SEM. (n = 3). (d) Gene expression profile of the investigated cells. (e) MEFs were transfected with expression plasmids or transduced with retroviruses for expression of *OCT4*, *SOX2*, or *NANOG*. *Mitf*, *Tyrp1*, *Trpm1*, and *Tyrosinase* mRNA levels were evaluated at day 6 post Dox induction. Levels were normalized to *Gapdh*. Fold changes relative to control cells transfected with empty vector (pcDNA) and treated with Dox are shown. Error bars represent ± SEM. * indicates $p < 0.05$, ** indicates $p < 0.01$ (n = 3). Experiment process is shown schematically to the right. (f) MEFs were transfected with a plasmid for expression of *OCT4* or empty vector control (pcDNA). Tyrosinase activity (Cy5, green) was evaluated at day 6 post Dox induction. Nuclei appear blue (DAPI). Green pixel quantification for 10 nuclei from each treatment using ImageJ software is plotted to the right. (g) mESCs were transduced with lentiviral vectors for expression of shRNA targeting *Oct4* or empty vector as control (sh-control). *Mitf*, *Tyrp2*, *Trpm1*, and *Tyrosinase* mRNA levels were evaluated at day 6 post Dox induction. Levels were normalized to *Gapdh*, and fold changes relative to control are shown. Error bars represent ± SEM (n = 2). Experiment process is presented schematically on the right.

Figure 4: OCT4 interferes with MITF transcriptional activity. (a) Pie chart representations of promoter regions occupied by MITF (upper panel) and of the realms which are engaged by MITF and OCT4 (lower panel). (b) Frequency of both OCT4 and MITF peaks within a given distance. (c) Illustration of MITF and OCT4 peak positions on *TRPM1* (upper panel) and *TYR* genes (lower panel). Regions upstream of transcription start sites are shown; numbers indicate the nucleotide position. The MITF binding motif (E-box: CATGTG) is shown in blue, and the OCT4 binding motif (Octamer box: NATGCAAN) is shown in red. (d) HEK293T cells were co-transfected with luciferase reporter driven by *TRPM1* or *TYR* promoter and plasmids for expression of MITF, wild-type OCT4 (OCT4_WT), mutated OCT4 (OCT4_MUT) or empty plasmid as control (upper panel). WM3682 cells were co-transfected with luciferase

reporter driven by *TRPM1* or *TYR* promoter and with a plasmid for expression of OCT4_WT, OCT4_MUT, or empty plasmid as control (lower panel). Luciferase activity was normalized to *Renilla* luciferase activity. Fold changes relative to control are shown. Error bars represent ± SEM, * indicates $p < 0.05$, ** indicates $p < 0.01$ ($n = 3$). (e) Left: WM3682 cells were transfected with vector for OCT4 expression or empty vector. *TRPM1* and *TYR* mRNA levels were evaluated 48 h post transfection. Levels were normalized to *GAPDH*, and fold changes relative to control are shown. Error bars represent ± SEM, * indicates $p < 0.05$ ($n = 3$). Right: WM3314 cells were transfected with vectors for expression of MITF and OCT4. *TRPM1* mRNA levels were evaluated 72 h post transfection. Levels were normalized to *GAPDH*, and fold changes relative to control are shown. Error bars represent ± SEM, * indicates $p < 0.05$ ($n = 3$). (f) Co-immunoprecipitation assay of MITF-HA and OCT4-flag. Samples were precipitated using anti-HA. Anti-HA or anti-flag were used for western blot. (g) EMSA was conducted using a probe corresponding to the E-box region of the human miR-211 promoter. HEK293T nuclear extracts were incubated with biotinylated probe. Bands corresponding to MITF binding and free probe are marked with arrows.

Figure 5: Oct4 maintains pluripotency and prevents differentiation. (a) Venn diagrams represent the number of gene promoters bound by OCT4 and lineage specific transcription factors based on ChIP-seq. (b) A view of the selected biological pathways identified by Gene Ontology enrichment analysis of genes bound by OCT4 and lineage-specific factors. (c) Melanocytes were generated from the epidermis and primary cells were extracted from brain, heart, and intestine of mice that inducibly express *Oct4*. (d) Levels of lineage-specific mRNAs in the indicated cell types at day 6 post Dox induction of *Oct4* expression relative to vehicle treated cells are shown. Levels were normalized to *Gapdh*. Error bars represent ± SEM. * indicates $p < 0.05$ ($n = 3$). (e) Overlap between OCT4 and indicated transcription factor peaks in Hi-C domains. Lineage specific transcription factors are highlighted in colors corresponding to the Venn diagrams in panel a. (f) Right: Hi-C map of human lymphoblastoid cells. RefSeq genes and ChIP-seq peaks of OCT4 and MITF are shown as green horizontal lines. Left: Chromosome 15 is magnified and the melanogenic marker TRPM1 is marked with blue square. TRPM1 is in the black highlighted domains. (g) Graphs show the number of unique and overlapping enhancer regions bound by MITF and OCT4 or by MITF and P53 based on ChIP-seq coordinates.

References

1 Takahashi, K. & Yamanaka, S. Induction of pluripotent stem cells from mouse embryonic and adult fibroblast cultures by defined factors. *cell* **126**, 663-676 (2006).

2 Masui, S. *et al.* Pluripotency governed by Sox2 via regulation of Oct3/4 expression in mouse embryonic stem cells. *Nature cell biology* **9**, 625-635 (2007).

3 Singh, V. K., Kalsan, M., Kumar, N., Saini, A. & Chandra, R. Induced pluripotent stem cells: applications in regenerative medicine, disease modeling, and drug discovery. *Frontiers in cell and developmental biology* **3**, 2, doi:10.3389/fcell.2015.00002 (2015).

4 Graf, T. & Enver, T. Forcing cells to change lineages. *Nature* **462**, 587-594 (2009).

5 Ladewig, J., Koch, P. & Brüstle, O. Leveling Waddington: the emergence of direct programming and the loss of cell fate hierarchies. *Nature reviews Molecular cell biology* **14**, 225-236 (2013).

6 Klimanskaya, I., Rosenthal, N. & Lanza, R. Derive and conquer: sourcing and differentiating stem cells for therapeutic applications. *Nature Reviews Drug Discovery* **7**, 131-142 (2008).

7 Thomson, J. A. *et al.* Embryonic stem cell lines derived from human blastocysts. *science* **282**, 1145-1147 (1998).

8 Guenther, M. G. *et al.* Chromatin structure and gene expression programs of human embryonic and induced pluripotent stem cells. *Cell Stem Cell* **7**, 249-257, doi:10.1016/j.stem.2010.06.015 (2010).

9 Yamane, T., Hayashi, S. I., Mizoguchi, M., Yamazaki, H. & Kunisada, T. Derivation of melanocytes from embryonic stem cells in culture. *Developmental Dynamics* **216**, 450-458 (1999).

10 Pla, P. *et al.* Dct:: lacZ ES cells: a novel cellular model to study melanocyte determination and differentiation. *Pigment cell research* **17**, 142-149 (2004).

11 Mica, Y., Lee, G., Chambers, S. M., Tomishima, M. J. & Studer, L. Modeling neural crest induction, melanocyte specification, and disease-related pigmentation defects in hESCs and patient-specific iPSCs. *Cell reports* **3**, 1140-1152 (2013).

12 Levy, C., Khaled, M. & Fisher, D. E. MITF: master regulator of melanocyte development and melanoma oncogene. *Trends in molecular medicine* **12**, 406-414 (2006).

13 Goding, C. R. Mitf from neural crest to melanoma: signal transduction and transcription in the melanocyte lineage. *Genes & Development* **14**, 1712-1728 (2000).

14 Steingrímsson, E., Copeland, N. G. & Jenkins, N. A. Melanocytes and the microphthalmia transcription factor network. *Annu. Rev. Genet.* **38**, 365-411 (2004).

15 Cheli, Y., Ohanna, M., Ballotti, R. & Bertolotto, C. Fifteen-year quest for microphthalmia-associated transcription factor target genes. *Pigment cell & melanoma research* **23**, 27-40 (2010).

16 Garraway, L. A. *et al.* Integrative genomic analyses identify MITF as a lineage survival oncogene amplified in malignant melanoma. *Nature* **436**, 117-122 (2005).

17 Goodall, J. *et al.* Brn-2 Represses Microphthalmia-Associated Transcription Factor Expression and Marks a Distinct Subpopulation of Microphthalmia-Associated Transcription Factor–Negative Melanoma Cells. *Cancer research* **68**, 7788-7794 (2008).

18 Tachibana, M. *et al.* Ectopic expression of MITF, a gene for Waardenburg syndrome type 2, converts fibroblasts to cells with melanocyte characteristics. *Nature genetics* **14**, 50-54 (1996).

19 Yang, R. *et al.* Direct conversion of mouse and human fibroblasts to functional melanocytes by defined factors. *Nature communications* **5** (2014).

20 Hochedlinger, K., Yamada, Y., Beard, C. & Jaenisch, R. Ectopic expression of Oct-4 blocks progenitor-cell differentiation and causes dysplasia in epithelial tissues. *Cell* **121**, 465-477 (2005).

21 Ferber, S. *et al.* Pancreatic and duodenal homeobox gene 1 induces expression of insulin genes in liver and ameliorates streptozotocin-induced hyperglycemia. *Nature medicine* **6**, 568-572, doi:10.1038/75050 (2000).

22 Zhou, Q., Brown, J., Kanarek, A., Rajagopal, J. & Melton, D. A. In vivo reprogramming of adult pancreatic exocrine cells to beta-cells. *Nature* **455**, 627-632, doi:10.1038/nature07314 (2008).

23 Nam, Y. J. *et al.* Reprogramming of human fibroblasts toward a cardiac fate. *Proc Natl Acad Sci U S A* **110**, 5588-5593, doi:10.1073/pnas.1301019110 (2013).

24 Kippenberger, S., Bernd, A., BEREITER-HAHN, J., RAMIREZ-BOSCA, A. & Kaufmann, R. The mechanism of melanocyte dendrite formation: the impact of differentiating keratinocytes. *Pigment cell research* **11**, 34-37 (1998).

25 Sarangarajan, R. & Boissy, R. E. Tyrp1 and oculocutaneous albinism type 3. *Pigment cell research* **14**, 437-444 (2001).

26 Dror, S. *et al.* Melanoma miRNA trafficking controls tumour primary niche formation. *Nature cell biology* **18**, 1006-1017, doi:10.1038/ncb3399 (2016).

27 Tachibana, M., Takeda, K., Nobukuni, Y. & Urabe, K. Ectopic expression of MITF, a gene for Waardenburg syndrome type 2, converts fibroblasts to cells with melanocyte characteristics. *Nature genetics* **14**, 50-54 (1996).

28 Hanna, J. *et al.* Direct reprogramming of terminally differentiated mature B lymphocytes to pluripotency. *Cell* **133**, 250-264 (2008).

29 Gaspar-Maia, A., Alajem, A., Meshorer, E. & Ramalho-Santos, M. Open chromatin in pluripotency and reprogramming. *Nature reviews Molecular cell biology* **12**, 36-47 (2011).

30 Radzisheuskaya, A. *et al.* A defined Oct4 level governs cell state transitions of pluripotency entry and differentiation into all embryonic lineages. *Nature cell biology* **15**, 579-590 (2013).

31 Wang, Z., Oron, E., Nelson, B., Razis, S. & Ivanova, N. Distinct lineage specification roles for NANOG, OCT4, and SOX2 in human embryonic stem cells. *Cell stem cell* **10**, 440-454 (2012).

32 Thomson, M. *et al.* Pluripotency factors in embryonic stem cells regulate differentiation into germ layers. *Cell* **145**, 875-889 (2011).

33 Angeletti, C., Khomitch, V., Halaban, R. & Rimm, D. L. Novel tyramide-based tyrosinase assay for the detection of melanoma cells in cytological preparations. *Diagn Cytopathol* **31**, 33-37, doi:10.1002/dc.20051 (2004).

34 Strub, T. *et al.* Essential role of microphthalmia transcription factor for DNA replication, mitosis and genomic stability in melanoma. *Oncogene* **30**, 2319-2332 (2011).

35 Gifford, C. A. *et al.* Transcriptional and epigenetic dynamics during specification of human embryonic stem cells. *Cell* **153**, 1149-1163, doi:10.1016/j.cell.2013.04.037 (2013).

36 Jin, V. X., O'Geen, H., Iyengar, S., Green, R. & Farnham, P. J. Identification of an OCT4 and SRY regulatory module using integrated computational and experimental genomics approaches. *Genome research* **17**, 807-817 (2007).

37 Brumbaugh, J. *et al.* Phosphorylation regulates human OCT4. *Proceedings of the National Academy of Sciences of the United States of America* **109**, 7162-7168, doi:10.1073/pnas.1203874109 (2012).

38 Tsankov, A. M. *et al.* Transcription factor binding dynamics during human ES cell differentiation. *Nature* **518**, 344-349 (2015).

39 Sugita, S. *et al.* Transcription factor Hes1 modulates osteoarthritis development in cooperation with calcium/calmodulin-dependent protein kinase 2. *Proceedings of the National Academy of Sciences* **112**, 3080-3085 (2015).

40 Vachtenheim, J. & Borovanský, J. "Transcription physiology" of pigment formation in melanocytes: central role of MITF. *Experimental dermatology* **19**, 617-627 (2010).

41 Kuo, C. T. *et al.* GATA4 transcription factor is required for ventral morphogenesis and heart tube formation. *Genes & development* **11**, 1048-1060 (1997).

42 Molkentin, J. D., Lin, Q., Duncan, S. A. & Olson, E. N. Requirement of the transcription factor GATA4 for heart tube formation and ventral morphogenesis. *Genes & development* **11**, 1061-1072 (1997).

43 Webster, D. E. *et al.* Enhancer-targeted genome editing selectively blocks innate resistance to oncokinase inhibition. *Genome research* **24**, 751-760, doi:10.1101/gr.166231.113 (2014).

44 Hochedlinger, K., Yamada, Y., Beard, C. & Jaenisch, R. Ectopic expression of Oct-4 blocks progenitor-cell differentiation and causes dysplasia in epithelial tissues. *Cell* **121**, 465-477, doi:10.1016/j.cell.2005.02.018 (2005).

45 Lieberman-Aiden, E. *et al.* Comprehensive mapping of long-range interactions reveals folding principles of the human genome. *Science* **326**, 289-293, doi:10.1126/science.1181369 (2009).

46 Dixon, J. R. *et al.* Topological domains in mammalian genomes identified by analysis of chromatin interactions. *Nature* **485**, 376-380, doi:10.1038/nature11082 (2012).

47 Nora, E. P. *et al.* Spatial partitioning of the regulatory landscape of the X-inactivation centre. *Nature* **485**, 381-385, doi:10.1038/nature11049 (2012).

48 Schoenfelder, S. *et al.* The pluripotent regulatory circuitry connecting promoters to their long-range interacting elements. *Genome research* **25**, 582-597 (2015).

49 Hakim, O. *et al.* Spatial congregation of STAT binding directs selective nuclear architecture during T-cell functional differentiation. *Genome research* **23**, 462-472 (2013).

50 Pope, B. D. *et al.* Topologically associating domains are stable units of replication-timing regulation. *Nature* **515**, 402-405, doi:10.1038/nature13986 (2014).

51 Weintraub, H. *et al.* Activation of muscle-specific genes in pigment, nerve, fat, liver, and fibroblast cell lines by forced expression of MyoD. *Proceedings of the National Academy of Sciences* **86**, 5434-5438 (1989).

52 Takahashi, K. & Yamanaka, S. Induction of pluripotent stem cells from mouse embryonic and adult fibroblast cultures by defined factors. *Cell* **126**, 663-676 (2006).

53 Chronis, C. *et al.* Cooperative Binding of Transcription Factors Orchestrates Reprogramming. *Cell* **168**, 442-459 e420, doi:10.1016/j.cell.2016.12.016 (2017).

54 Kushwaha, R. *et al.* Interrogation of a context-specific transcription factor network identifies novel regulators of pluripotency. *Stem Cells* **33**, 367-377, doi:10.1002/stem.1870 (2015).

55 Beard, C., Hochedlinger, K., Plath, K., Wutz, A. & Jaenisch, R. Efficient method to generate single-copy transgenic mice by site-specific integration in embryonic stem cells. *Genesis* **44**, 23-28 (2006).

56 Saura, J., Tusell, J. M. & Serratosa, J. High-yield isolation of murine microglia by mild trypsinization. *Glia* **44**, 183-189 (2003).

57 Song, W., Lu, X. & Feng, Q. Tumor necrosis factor-α induces apoptosis via inducible nitric oxide synthase in neonatal mouse cardiomyocytes. *Cardiovascular research* **45**, 595-602 (2000).

58 Miller, A. J. *et al.* Transcriptional regulation of the melanoma prognostic marker melastatin (TRPM1) by MITF in melanocytes and melanoma. *Cancer research* **64**, 509-516 (2004).

59 Angeletti, C., Khomitch, V., Halaban, R. & Rimm, D. L. Novel tyramide-based tyrosinase assay for the detection of melanoma cells in cytological preparations. *Diagnostic cytopathology* **31**, 33-37 (2004).

60 Rao, S. S. *et al.* A 3D map of the human genome at kilobase resolution reveals principles of chromatin looping. *Cell* **159**, 1665-1680, doi:10.1016/j.cell.2014.11.021 (2014).

61 Consortium, E. P. An integrated encyclopedia of DNA elements in the human genome. *Nature* **489**, 57-74, doi:10.1038/nature11247 (2012).

62 Ernst, J. *et al.* Mapping and analysis of chromatin state dynamics in nine human cell types. *Nature* **473**, 43-49, doi:10.1038/nature09906 (2011).

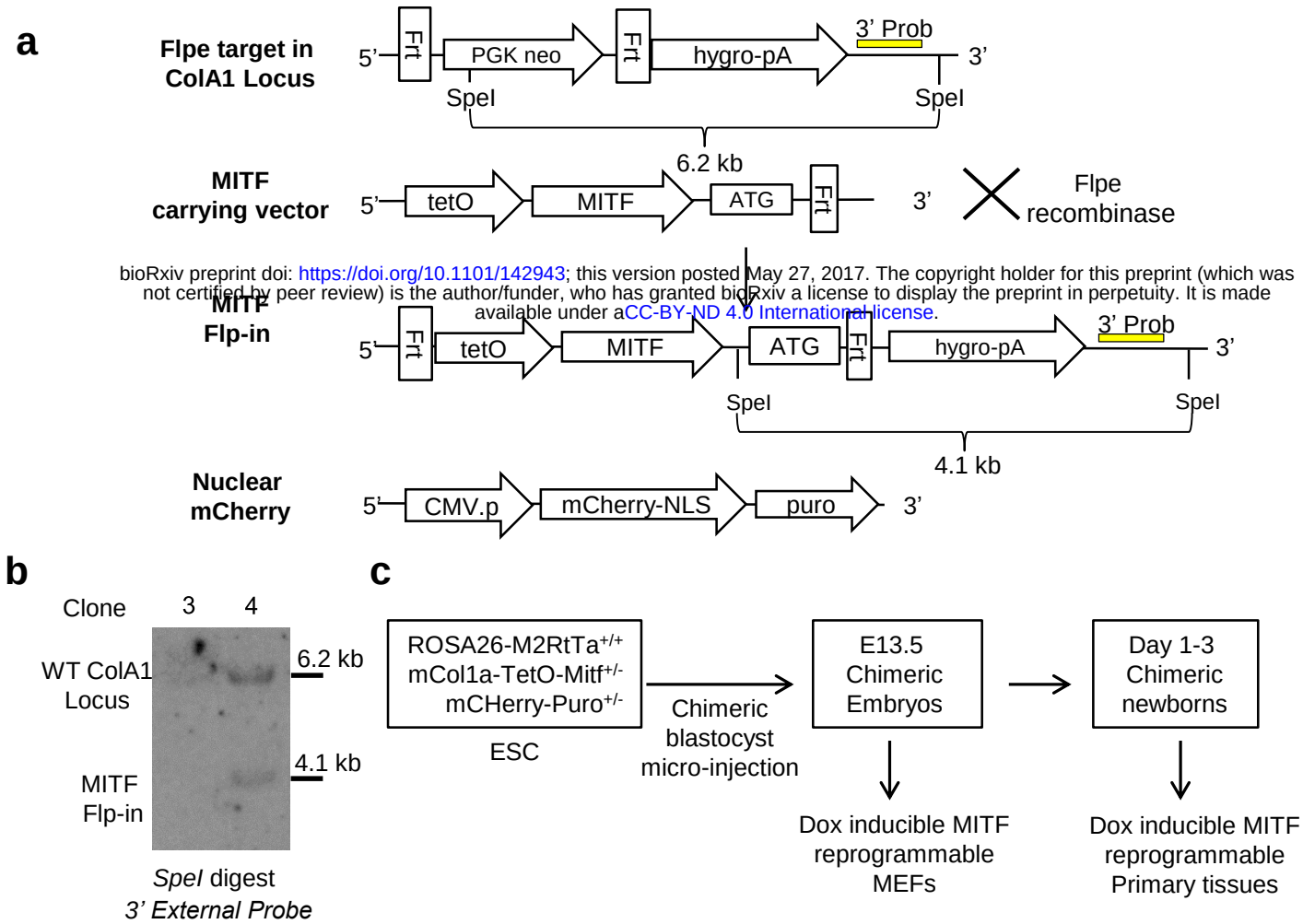

Figure 1: Generation of doxycycline-inducible Mitf knock-in reprogrammable system **Sheinboim et al**

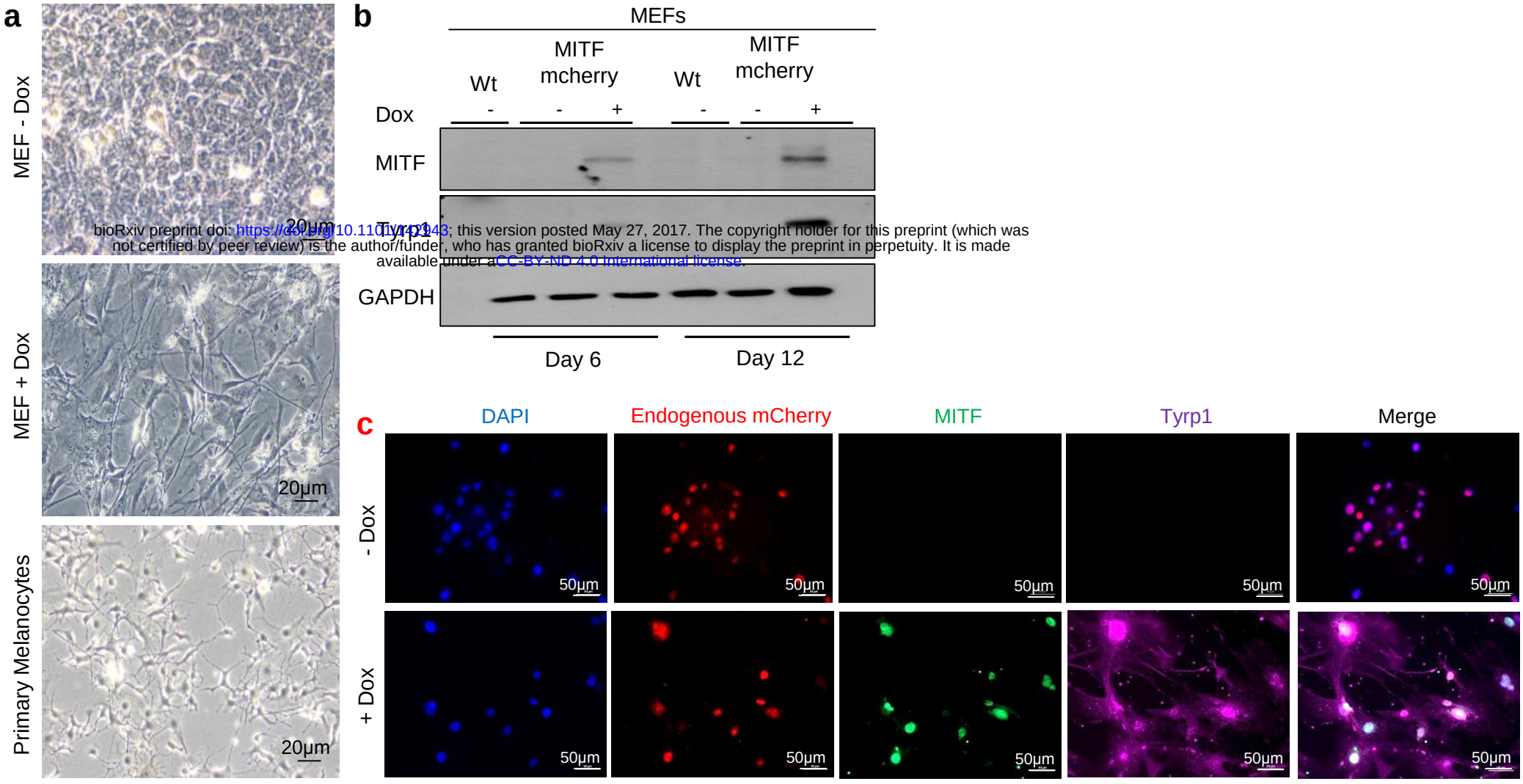

Figure 2: Highly efficient transdifferentiation of MEFs into melanocyte-like cells by MITF

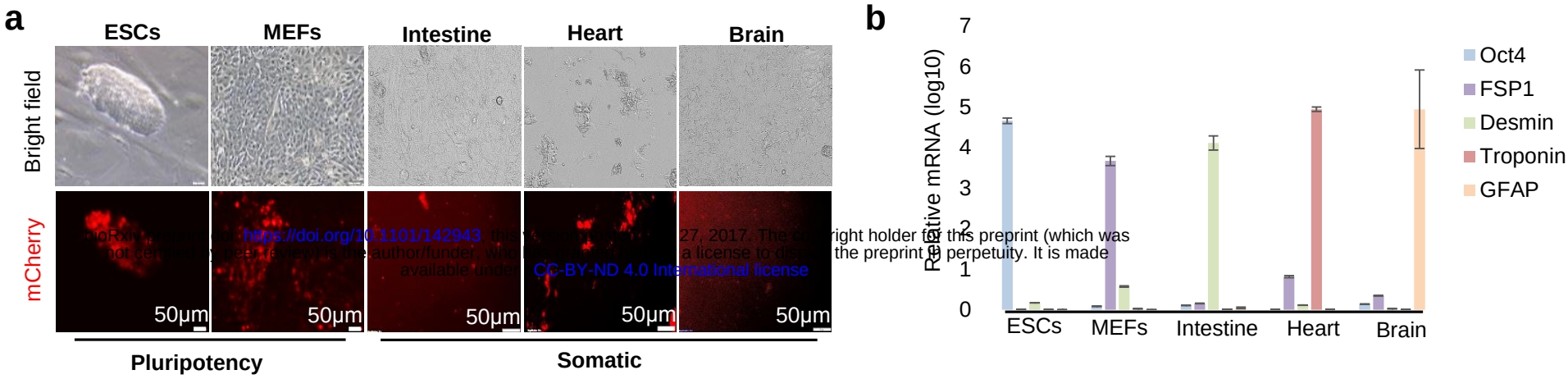

Figure 3: OCT4 impedes differentiation in ESCs despite Mitf expression

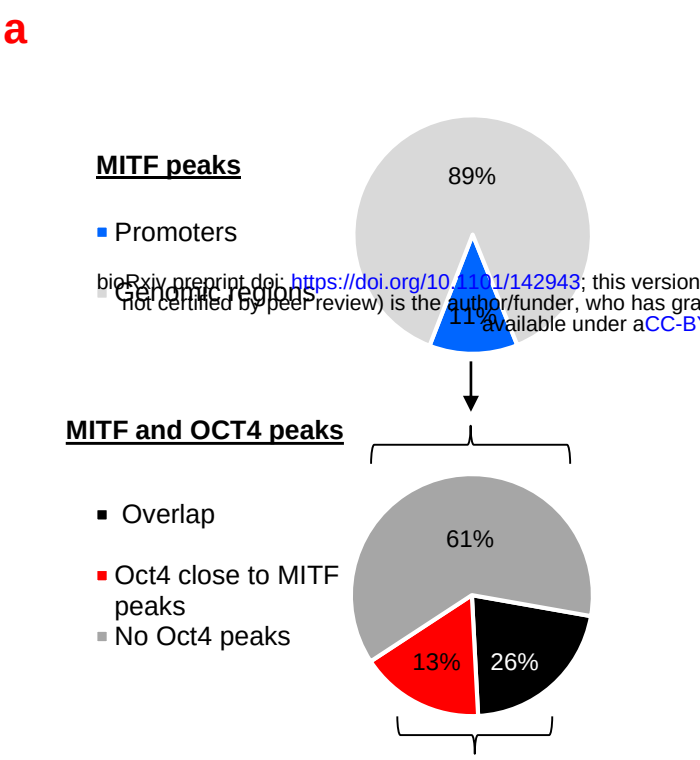

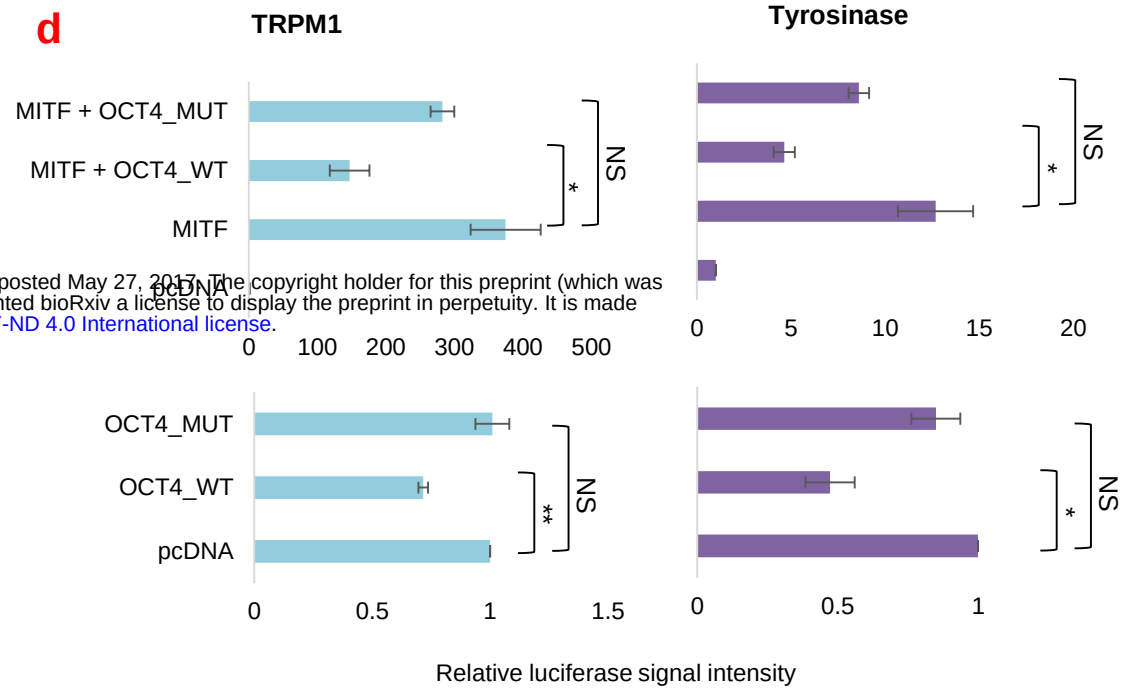

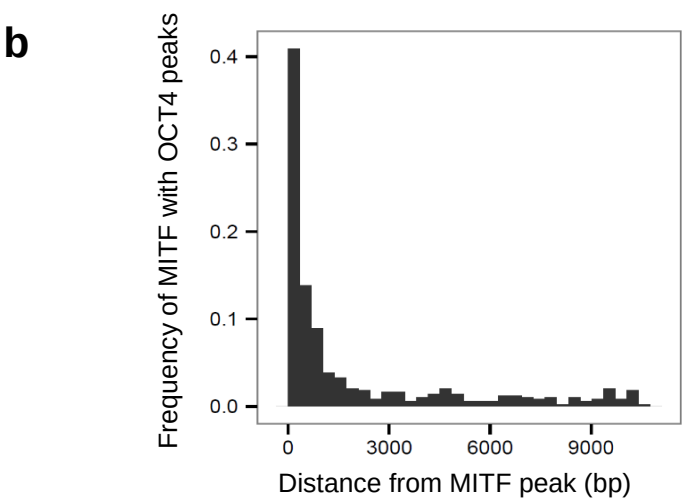

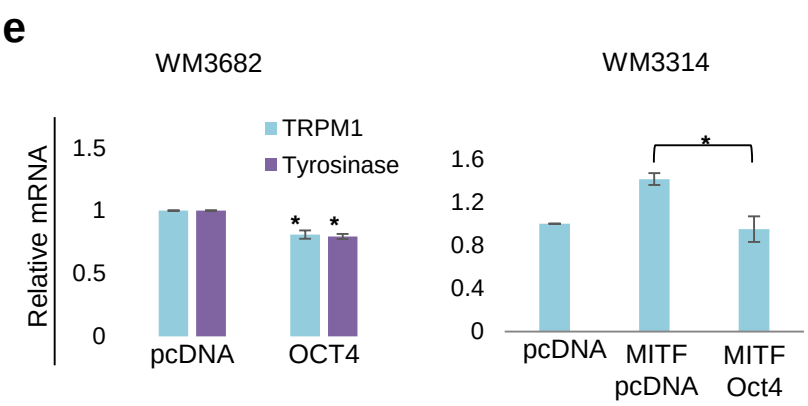

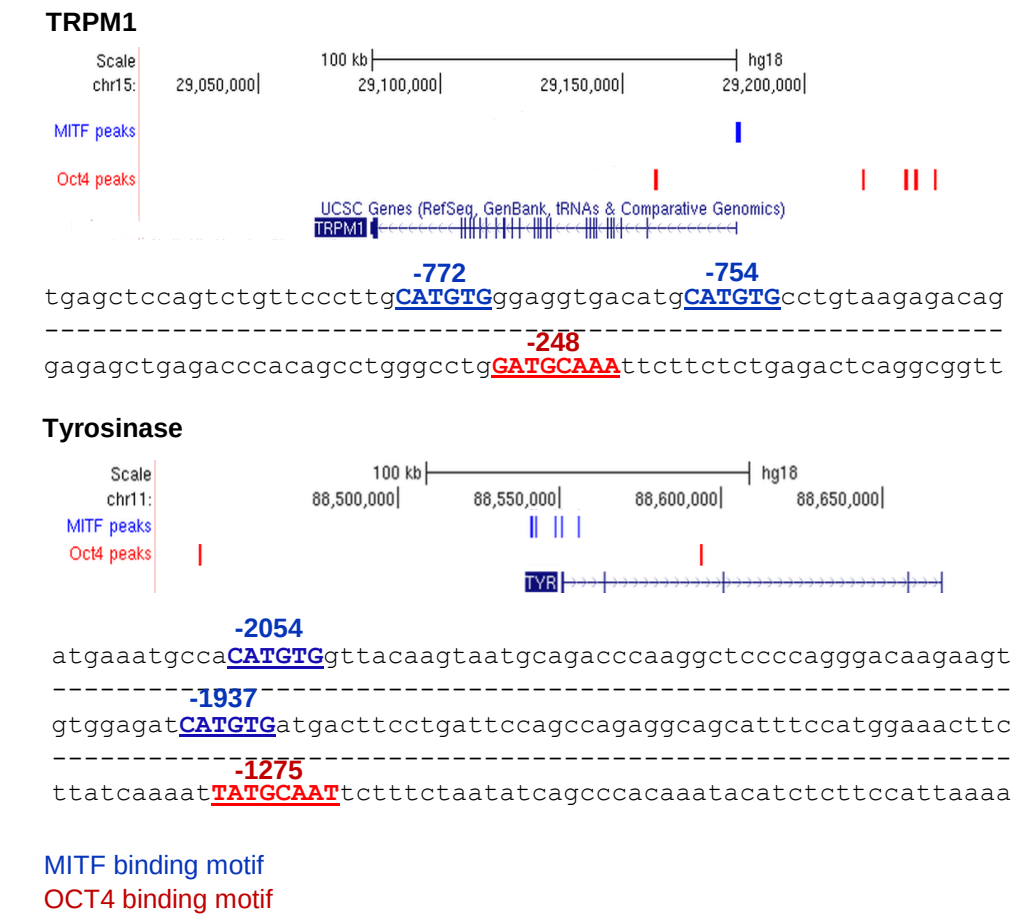

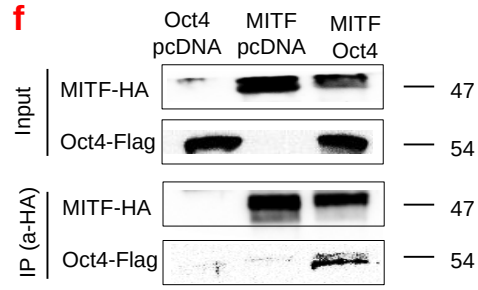

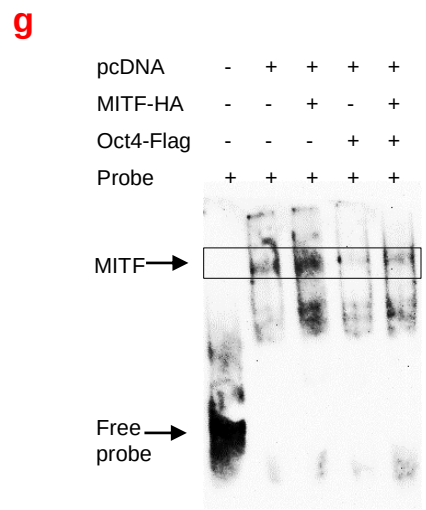

Figure 4: OCT4 interferes with MITF transcriptional activity

Figure 5: OCT4 maintains pluripotency and prevents differentiation